

Operando Electrochemical Liquid-Cell Scanning Transmission Electron Microscopy (EC-STEM) Studies of Evolving Cu Nanocatalysts for CO₂ Electroreduction

Yao Yang,* Yu-Tsun Shao, Jianbo Jin, Julian Feijóo, Inwhan Roh, Sheena Louisia, Sunmoon Yu, Maria V. Fonseca Guzman, Chubai Chen, David A. Muller, Héctor D. Abruña,* and Peidong Yang*



Cite This: <https://doi.org/10.1021/acssuschemeng.2c06542>



Read Online

ACCESS |



Metrics & More



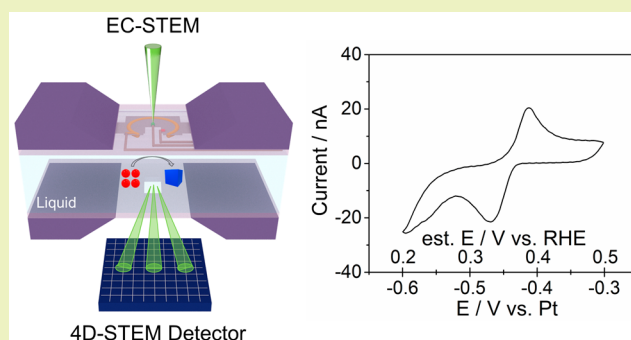
Article Recommendations



Supporting Information

ABSTRACT: The design and synthesis of nanocatalysts with well-defined sizes, compositions, and structures have revolutionized our accessibility to tunable catalyst activity and selectivity for a variety of energy-related electrochemical reactions. Nonetheless, establishing structure-(re)activity correlations requires the understanding of the dynamic evolution of pristine nanocatalysts and the identification of their active states under operating conditions. We previously communicated the *operando* observation of Cu nanocatalysts evolving into active metallic Cu nanograins for CO₂ electroreduction (Yang et al. *Nature* 2023, 614, 262–269). Here, we expand our discussion to the technical capabilities and further research applications of *operando* electrochemical liquid-cell scanning transmission electron microscopy (EC-STEM), which enables quantitative electrochemistry while tracking dynamic structural evolution of sub-10 nm Cu nanocatalysts. The coexistent H₂ bubbles, often disruptive to *operando* spectroscopy, are an effective approach to create a thin-liquid layer that significantly improves spatial resolution while remaining electrochemically accessible to Cu nanocatalysts. *Operando* four-dimensional (4D) STEM in liquids provides insights into the complex structure of active polycrystalline metallic Cu nanograins. With continuous technical developments, we anticipate that *operando* EC-STEM will evolve into a powerful electroanalytical method to advance our understanding of a variety of nanoscale electrocatalysts at solid/liquid interfaces.

KEYWORDS: *Operando*, EC-STEM, 4D-STEM, CO₂RR, Dynamic evolution, Cu nanocatalysts



INTRODUCTION

Electrocatalysis is the cornerstone of sustainable electrochemical energy technologies with the potential to significantly mitigate the environmental impacts of fossil fuels. Although conventional *ex situ* characterizations provide a baseline understanding, many nanoscale electrocatalysts undergo significant structural transformation under electrochemical reactions, which calls for the use of *operando/in situ* methods.^{1–7} In particular, the dynamic evolution of highly active Cu nanocatalysts under the CO₂ reduction reaction (CO₂RR) conditions requires nanoscale time-resolved analytical techniques.⁸ Cu nanocatalysts (sub-10 nm) were previously reported to selectively convert CO₂ to multicarbon (C₂₊) products at lower overpotentials (−0.8 vs reversible hydrogen electrode, RHE), than bulk Cu counterparts.⁹ In our recent work, a suite of *operando* electron microscopy and X-ray methods was employed to identify the structure of the active sites in Cu nanocatalysts as “Cu nanograins”.¹ At CO₂RR operating potentials, the hydrogen evolution reaction (HER) accounts for a significant fraction of the Faradaic efficiency.

The H₂ bubbles, generated along with the CO₂RR, often pose a significant challenge for *operando* vibrational spectroscopy and X-ray absorption spectroscopy that require a stable liquid thickness for background subtraction in spectroscopic analysis.⁴ Electrochemical liquid-cell scanning transmission electron microscopy (EC-STEM) cells have a liquid thickness of 500 nm or thicker at different locations of the cell due to the bulging out of the SiN_x windows in order to adjust to the pressure difference between the liquid cell and the TEM chamber.¹⁰ With such a thick liquid layer, the spatial resolution of STEM imaging in liquids is severely compromised, which makes it particularly challenging to resolve sub-10 nm features at a beam dose below the threshold of affecting electro-

Received: November 1, 2022

Revised: February 10, 2023

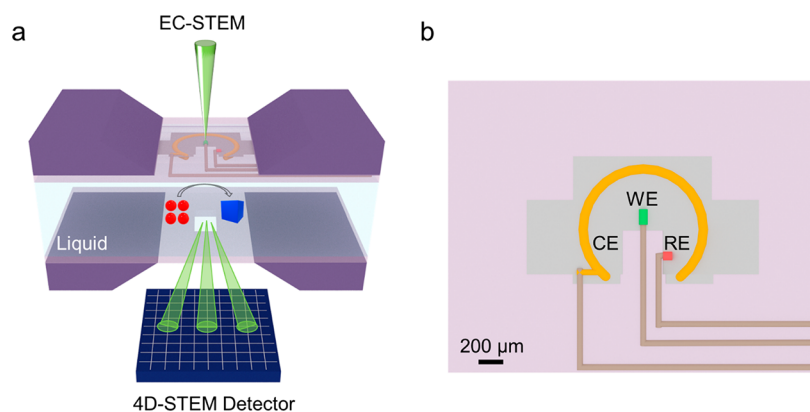


Figure 1. (a) Schematic of *Operando* EC-STEM with a 4D-STEM detector that enables reliable electrochemistry while monitoring dynamic morphological and structural changes under electrocatalytically relevant conditions. (b) Schematic of the three-electrode system with nanocatalysts deposited on the working electrode (WE) and Pt counter and pseudoreference electrodes (CE and pseudo-RE, respectively).

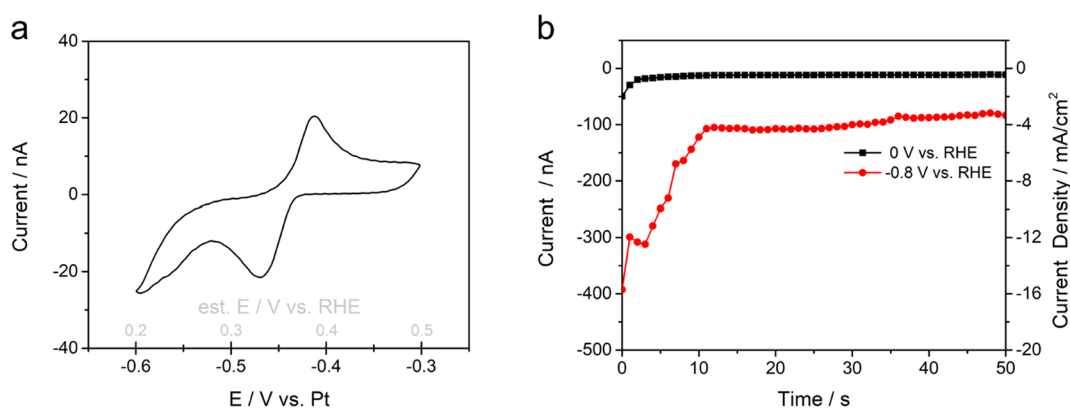


Figure 2. (a) CV profile of a 7 nm Cu NP ensemble on the carbon WE in CO_2 -saturated 0.1 M KHCO_3 at 100 mV/s. (b) Corresponding CA profiles at 0 and -0.8 V vs RHE with current and current density as the left and right Y-axes, respectively.

chemical reactions.¹¹ The thick liquid also poses a formidable challenge to the use of electron diffraction for structural information in liquids.^{12–14} Our previous studies introduced the “thin-liquid” strategy enabled by H_2 bubbles electro-generated during cathodic corrosion, which enabled the first four-dimensional (4D) STEM diffraction imaging in liquids.¹⁵ In this *operando* EC-STEM study, we take advantage of the coexistent H_2 bubbles formed during the CO_2 RR to create a thin-liquid layer, which significantly improves spatial resolution for resolving dynamic evolution at the nanometer scale. 4D-STEM diffraction imaging is readily accessible in thin-liquid films to provide structural information on the polycrystalline metallic Cu nanograins. In the end, we identified several key aspects that are required to enable more quantitative electrochemistry in EC-STEM, so that this fast-growing technique can make significant contributions to the vast energy materials community, in general, and the electrocatalysis community, in particular.

RESULTS AND DISCUSSION

Operando EC-STEM enables quantitative electrochemistry and simultaneous tracking of the dynamic evolution of nanoscale electrocatalysts under operating conditions (Figure 1a). The electrochemical liquid cell is composed of a liquid layer with a 500 nm spacer in between two silicon nitride (SiN_x) windows (each is about 50 nm thick).^{16,17} The three-electrode system includes an electron-transparent and electrochemically inert

glassy carbon working electrode (WE) with a thickness of ~ 50 nm and geometric area of $\sim 2,500 \mu\text{m}^2$ (Figure 1b). The Pt counter electrode (CE) with a large area of 0.29 mm^2 , relative to the WE, enables a rapid polarization in response to the applied potential on the WE. The circular CE can establish a symmetrical electrical field and uniform current density around the WE and is positioned sufficiently far away from the WE to minimize the effects of electrochemical reactions of the CE on the WE. Given the sub-micrometer electrolyte, it is challenging to accommodate a standard RE such as Ag/AgCl in the KCl solution with a salt bridge within the liquid cell. Pt serves as a pseudo-RE for its chemical stability, wide potential window, and facile nanofabrication.

A 7 nm Cu nanoparticle NP ensemble was deposited on the glassy carbon WE for electrochemical measurements in CO_2 -saturated 0.1 M KHCO_3 . The as-synthesized NP ensemble rapidly oxidizes to Cu_2O after brief air exposure prior to electrochemical reactions.¹ The cyclic voltammetric (CV) profile of the 7 nm Cu NP ensemble shows well-defined reduction and oxidation peaks, corresponding to Cu_2O reduction to Cu and Cu reoxidation to Cu_2O , respectively (Figure 2a). The electroreduction peak of the NP ensemble is located at ~ 0.35 V vs RHE, which is consistent with the reduction peak of NP ensembles measured in a standard electrochemical H-cell at ~ 0.45 V vs RHE (Figure S1a). The discrepancy may come from the uncertainty in potential conversion given that the potential of the Pt pseudo reference electrode (pseudo-RE) is estimated to be 0.8 ± 0.1 V vs the

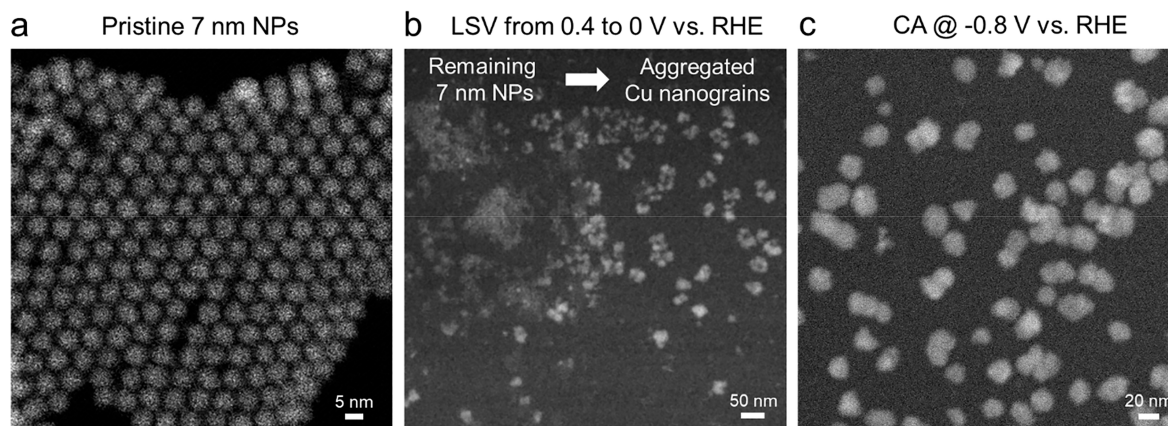


Figure 3. Dynamic evolution of the 7 nm NP ensemble under CO₂RR relevant conditions. (a) HAADF-STEM image of the monolayer NP ensemble. (b) *Operando* EC-STEM images capturing both the remaining 7 nm NPs and the initial formation of loosely connected Cu nanograins after an LSV scan from 0.4 to 0 V vs RHE. (c) *Operando* EC-STEM image of the steady-state formation of closely packed Cu nanograins after CA at -0.8 V vs RHE.

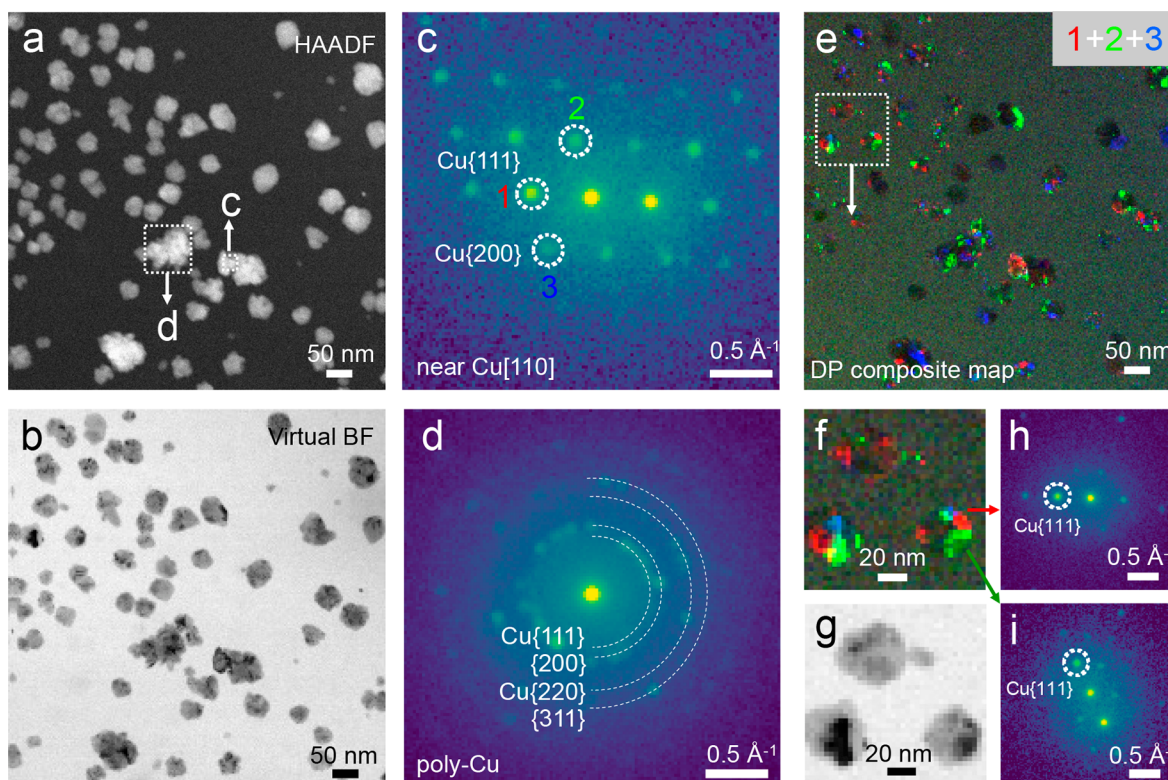


Figure 4. *Operando* electrochemical 4D-STEM diffraction imaging of Cu nanograins generated at -0.8 V vs RHE. (a-b) HAADF-STEM image and corresponding virtual BF-STEM image extracted from the central disk in the 4D-STEM data set. (c-d) Representative diffraction patterns near the Cu[110] zone axis and polycrystalline Cu of Cu nanograins labeled in (a). (e) False-color dark-field 4D-STEM composite images showing polycrystalline Cu nanograins extracted from diffraction spots marked as 1 (red), 2 (green), and 3 (blue), respectively, in (c). (f-g) Magnified region from the dashed box in (e) and (g) corresponding to the virtual BF-STEM image. (h-i) Diffraction patterns corresponding to Cu domains 1 (red) and 2 (green) in (f), respectively.

reversible hydrogen electrode (RHE).^{1,4} The chronoamperometric (CA) profile of the Cu NP ensemble at 0 V vs RHE simulates the operating conditions near the hydrogen evolution reaction (HER) with a steady-state current of about -10 nA (Figure 2b). The CA profile at -0.8 V vs RHE simulates the optimal CO₂RR potential for C₂₊ formation on a 7 nm NP ensemble⁹ and shows a stable current plateau of about -100 nA (about -4 mA/cm² by normalizing the current to the geometric area of the WE). This is within the same order of

magnitude as the operating current density in a realistic electrochemical H-cell (about -14 mA/cm²) at -0.8 V vs RHE (Figure S1b). The ohmic resistance was measured to be 20–30 kΩ in the 0.1 M KHCO₃ electrolyte with electrochemical impedance spectroscopy (EIS). Given the ~ 100 nA operating current in EC-STEM, the *iR* drop was estimated to be 2–3 mV, a negligible value when compared to the operating potential. In summary, these electrochemical measurements indicate that *operando* EC-STEM is capable of delivering a

comparable reaction rate (current density) at a comparable driving force (applied potential; overpotential), relative to standard electrochemical measurements.

Operando EC-STEM under CO₂RR relevant conditions makes use of the electrogenerated H₂ bubbles to generate a thin-liquid layer with significantly enhanced spatial resolution. With linear sweep voltammetry (LSV) from 0.4 to around 0 V vs RHE, H₂ gas bubbles are formed (Figure S2). An initial potential below the open circuit potential (OCP) at about 0.6 V vs RHE was chosen in order to start with a reducing current and avoid undesirable structural changes due to oxidation from Cu₂O to CuO at more positive potentials. As the LSV reaches around 0 V vs RHE, the thick liquid layer is displaced, and dynamic particle aggregation is clearly resolved (Figure S2c). In an effort to determine the thickness of the thin-liquid layer, low-loss electron energy loss spectroscopy (EELS) was performed and analyzed based on Beer's law (Figure S3).^{10,18} The thickness of the dry SiN_x windows was measured to be about 100 nm, which is consistent with the combined thickness of two layers of 50 nm-thick SiN_x windows. The total thickness of the thin-liquid layer and the SiN_x windows was measured to be 200 ± 15 nm (Table S1). Thus, the estimated thickness of the thin-liquid layer is about 100 nm. Assuming that the liquid layer has the same thickness below and above the H₂ bubbles within the cell, the liquid covering the WE is about 50 nm thick. It should be noted that both CA profiles at 0 and -0.8 V vs RHE were acquired after H₂ bubble formation (Figure 2b). The stable current plateau with mA/cm²-level current density at -0.8 V vs RHE suggests that the hydrophilic glassy carbon WE, covered with a thin-liquid layer, remains electrochemically accessible to the CO₂RR instead of drying out after forming H₂ bubbles.

With electrochemical measurements and liquid thickness quantification established, *operando* EC-STEM imaging was performed to investigate the dynamic morphological changes of Cu NPs under CO₂RR relevant conditions. Figure 3 provides an overview of the transformation of the 7 nm Cu NP ensemble under applied potentials. The high-angle annular dark-field detector (HAADF) STEM image shows that the as-synthesized 7 nm Cu NPs are monodisperse and self-assembled in a hexagonal packing on the carbon substrate (Figure 3a). The interparticle distance was estimated to be ~1 nm based on our previous resonant soft X-ray scattering study.¹⁹ After the LSV scan from 0.4 to 0 V vs RHE, the *operando* EC-STEM image in Figure 3b captures both the remaining 7 nm Cu NPs on the left and the initial aggregation into loosely connected Cu nanograins (Figures S4, S5). No beam damage was observed at a low beam dose of ~50 e⁻/nm² per image frame (dose rate of ~12.5 e⁻/nm² s).⁹ Under CO₂RR relevant conditions (-0.8 V vs RHE), those newly formed Cu nanograins undergo further aggregation/coalescence and reach a steady-state structure of closely packed Cu nanograins (50–100 nm, Figures 3, 4a). Detailed analysis of *operando* EC-STEM movies of dynamic evolution can be found in our recent work.¹

With the thin-liquid strategy, this study can go beyond conventional STEM imaging and enable 4D-STEM diffraction imaging in liquids. The 4D-STEM data set is captured on an electron microscopy pixel array detector (EMPAD) with single electron sensitivity and fast readout speed^{20,21} which are crucial for low-dose electron diffraction in beam-sensitive liquids.^{1,15} 4D-STEM diffraction imaging was acquired at an estimated beam dose of ~2,000 e⁻/nm² (a dose rate of ~6 e⁻/

nm² s). The HAADF-STEM image shows that irregular Cu nanograins (50–100 nm) are formed at -0.8 V vs RHE under CO₂RR relevant conditions (Figure 4a). A virtual bright-field (BF) STEM image was reconstructed by integrating the (000) transmitted spot of the 4D-STEM data set which shows the granular features of those Cu nanograins (Figure 4b). Two representative diffraction patterns were selected to show the different orientations of the Cu nanograins (Figure 4c,d). Some regions of the Cu nanograins show a diffraction pattern with Cu{111} (2.1 Å) and Cu{200} (1.8 Å) spots near the Cu[110] zone axis (Figure 4c). However, the vast majority of the Cu nanograins shows highly polycrystalline diffraction patterns like the one in Figure 4d. A false-color dark-field 4D-STEM composite image (Figure 4e), extracted from three diffraction spots (1 (red), 2 (green), and 3 (blue)) in Figure 4c, shows crystal domains matching crystal orientations of those three diffraction spots. The magnified composite image and corresponding virtual BF-STEM image (Figure 4f,g), as well as diffraction patterns in Figure 4h,l, better illustrate that multiple Cu nanograins with different crystal orientations can exist within each particle.

In summary, this study illustrates the electrochemical capability of *operando* EC-STEM and presents the application of the "thin-liquid" strategy enabled by electrogenerated H₂ bubbles under CO₂RR conditions. The pristine 7 nm Cu NP ensemble undergoes a dramatic structural transformation into an active state of polycrystalline metallic Cu nanograins (50–100 nm). *Operando* electrochemical 4D-STEM structural analysis provides a glimpse into the complex nature of active metallic Cu nanograins under CO₂RR conditions. Future work on quantifying grain sizes and density may provide additional insights into how to tune the structure of Cu nanograins for more effective C–C coupling reactions. This study points out the need for *operando* methods to investigate active sites of electrocatalysts instead of relying on conventional *ex situ* methods, especially for highly reactive Cu nanocatalysts.^{22–24} We would also like to point out several future directions that are required to make *operando* EC-STEM more accessible to the broad energy materials community.

- (1) **Quantification of applied potentials.** A rigorous calibration of the potential of the Pt pseudo-RE in different electrolyte environments will be instrumental to benchmark electrochemistry in *operando* EC-STEM. The uncertainty of the Pt pseudo-RE potential values (~0.1 V) is less of an issue for electrochemical reactions such as the CO₂RR, N₂ electroreduction, or oxygen evolution reaction (OER) that require significantly large overpotentials to operate. However, a stable RE with an uncertainty below 10 mV will be required to study electrochemical reactions that are highly sensitive to small changes in overpotentials, in particular, hydrogen oxidation/evolution reactions (HOR/HER) and the oxygen reduction reaction (ORR) for fuel cells. In comparison, a commercial RE electrode, such as Ag/AgCl or Hg/HgO, can connect to the liquid cell externally and serve as a stable potential reference point with a stability of the order of 1 mV.^{25,26} We anticipate that the incorporation of a more stable RE will be critical to enable more quantitative electrochemistry, so that EC-STEM can evolve into a reliable *operando* electrochemical technique, like *operando* X-ray absorption spectroscopy, that can be widely and readily used by

electrochemists to investigate electrochemical reaction dynamics with unprecedented spatiotemporal resolutions.

- (2) **Quantification of current density.** Preliminary comparison of the average current density on a glassy carbon WE in EC-STEM, and that in standard electrochemical cells, suggests that the reaction rates are on the same order of magnitude. The current density, normalized to the geometric area of the WE, only reveals limited information about intrinsic reaction rates. Quantification of the electrochemical surface area (ECSA) of electrocatalysts in EC-STEM will be critical to provide information on intrinsic activity per active sites and potential-dependent surface coverage of reaction intermediates. Modeling of the electric field distribution of the WE can advance our understanding of the reaction rate as a function of applied potentials, electrolyte, adsorbates, and types of substrates, among others.²⁷ In particular, the heterogeneity in electric field distributions may have a strong effect on the reaction kinetics in the particularly thin-liquid layer.
- (3) **Improvement of spatial resolution without forming bubbles.** How can we expand *operando* EC-STEM to electrochemical reactions that do not generate H₂ bubbles, such as the HOR and ORR as well as in most battery applications?^{28–30} There is a need to push the technical limit of nanofabrication for a pristine liquid layer thickness on the order of 100 nm and thinner SiN_x windows.

■ ASSOCIATED CONTENT

SI Supporting Information

The Supporting Information is available free of charge at <https://pubs.acs.org/doi/10.1021/acssuschemeng.2c06542>.

Experimental methods (NP synthesis, *operando* EC-STEM and 4D-STEM measurements); Figures S1–S5 and Table S1, additional electrochemical, EC-STEM and EELS measurements (PDF)

■ AUTHOR INFORMATION

Corresponding Authors

Yao Yang – Department of Chemistry, University of California, Berkeley, California 94720, United States; Miller Institute for Basic Research in Science, University of California, Berkeley, California 94720, United States; Chemical Sciences Division, Lawrence Berkeley National Laboratory, Berkeley, California 94720, United States; orcid.org/0000-0003-0321-3792; Email: yaoyang1@berkeley.edu

Héctor D. Abuña – Kavli Institute at Cornell for Nanoscale Science and Department of Chemistry and Chemical Biology, Cornell University, Ithaca, New York 14853, United States; orcid.org/0000-0002-3948-356X; Email: hda1@cornell.edu

Peidong Yang – Department of Chemistry, University of California, Berkeley, California 94720, United States; Chemical Sciences Division, Lawrence Berkeley National Laboratory, Berkeley, California 94720, United States; Department of Materials Science and Engineering, University of California, Berkeley, California 94720, United States; Kavli Energy NanoScience Institute, Berkeley, California

94720, United States; orcid.org/0000-0003-4799-1684; Email: p_yang@berkeley.edu

Authors

Yu-Tsun Shao – School of Applied and Engineering Physics, Cornell University, Ithaca, New York 14853, United States

Jianbo Jin – Department of Chemistry, University of California, Berkeley, California 94720, United States; orcid.org/0000-0002-9054-7960

Julian Feijóo – Department of Chemistry, University of California, Berkeley, California 94720, United States; Chemical Sciences Division, Lawrence Berkeley National Laboratory, Berkeley, California 94720, United States

Inwhan Roh – Department of Chemistry, University of California, Berkeley, California 94720, United States; Chemical Sciences Division, Lawrence Berkeley National Laboratory, Berkeley, California 94720, United States; orcid.org/0000-0001-7337-4458

Sheena Louisia – Department of Chemistry, University of California, Berkeley, California 94720, United States; Chemical Sciences Division, Lawrence Berkeley National Laboratory, Berkeley, California 94720, United States; orcid.org/0000-0002-2175-6769

Sunmoon Yu – Chemical Sciences Division, Lawrence Berkeley National Laboratory, Berkeley, California 94720, United States; Department of Materials Science and Engineering, University of California, Berkeley, California 94720, United States; orcid.org/0000-0001-7250-9365

Maria V. Fonseca Guzman – Department of Chemistry, University of California, Berkeley, California 94720, United States; Chemical Sciences Division, Lawrence Berkeley National Laboratory, Berkeley, California 94720, United States

Chubai Chen – Department of Chemistry, University of California, Berkeley, California 94720, United States; Chemical Sciences Division, Lawrence Berkeley National Laboratory, Berkeley, California 94720, United States; orcid.org/0000-0003-2513-2707

David A. Muller – School of Applied and Engineering Physics, Cornell University, Ithaca, New York 14853, United States; Kavli Institute at Cornell for Nanoscale Science, Cornell University, Ithaca, New York 14853, United States; orcid.org/0000-0003-4129-0473

Complete contact information is available at: <https://pubs.acs.org/doi/10.1021/acssuschemeng.2c06542>

Notes

The authors declare no competing financial interest.

■ ACKNOWLEDGMENTS

This work was supported by the Director, Office of Science, Office of Basic Energy Sciences, Chemical Sciences, Geosciences, & Biosciences Division, of the US Department of Energy under Contract DE-AC02-05CH11231, FWP CH030201 (Catalysis Research Program). *Operando* EC-STEM was supported by the Center for Alkaline-Based Energy Solutions (CABES), an Energy Frontier Research Center (EFRC) program supported by the U.S. Department of Energy, under grant DE-SC0019445. This work made use of TEM facilities at the CCMR which are supported through the National Science Foundation Materials Research Science and Engineering Center (NSF MRSEC) program (DMR-1719875). This work also used TEM facilities at the Molecular

Foundry supported by the Office of Science, Office of Basic Energy Sciences, of the U.S. Department of Energy under Contract No. DE-AC02-05CH11231. Y.Y. acknowledges the support from the Miller Research Fellowship. J.J. and C.C. acknowledge the support from the Suzhou Industrial Park Scholarship. S.Y. acknowledges support from the Samsung Scholarship.

DEDICATION

We dedicate this work to Prof. Héctor Abruña's 70th birthday and over 40 years of contributions to *Operando* Electrochemistry.

REFERENCES

- (1) Yang, Y.; Louisia, S.; Yu, S.; Jin, J.; Roh, I.; Chen, C.; Fonseca Guzman, M. V.; Feijoo, J.; Chen, P.; Wang, H.; Pollock, C. J.; Huang, X.; Shao, Y.-T.; Wang, C.; Muller, D. A.; Abruña, H. D.; Yang, P. *Operando* Studies Reveal Active Cu Nanograins for CO₂ Electroreduction. *Nature* **2023**, *614*, 262–269.
- (2) Abruña, H. D.; Bommarito, G. M.; Acevedo, D. The Study of Solid/Liquid Interfaces with X-ray Standing Waves. *Science* **1990**, *250*, 69–74.
- (3) Abruña, H. D. *Electrochemical Interface: Modern Techniques for In Situ Interface Characterization*; VCH: New York, 1991.
- (4) Yang, Y.; Xiong, Y.; Zeng, R.; Lu, X.; Krumov, M.; Huang, X.; Xu, W.; Wang, H.; DiSalvo, F. J.; Brock, J. D.; Muller, D. A.; Abruña, H. D. *Operando* Methods in Electrocatalysis. *ACS Catal.* **2021**, *11*, 1136–1178.
- (5) Weckhuysen, B. M. Snapshots of a Working Catalyst: Possibilities and Limitations of *In Situ* Spectroscopy in the Field of Heterogeneous Catalysis. *Chem. Commun.* **2002**, 97–110.
- (6) Bañares, M. A. *Operando* Methodology: Combination of *In Situ* Spectroscopy and Simultaneous Activity Measurements under Catalytic Reaction Conditions. *Catal. Today* **2005**, *100*, 71–77.
- (7) Williamson, M.; Tromp, R.; Vereecken, P.; Hull, R.; Ross, F. Dynamic Microscopy of Nanoscale Cluster Growth at the Solid-Liquid Interface. *Nat. Mater.* **2003**, *2*, 532–536.
- (8) Li, Y.; Kim, D.; Louisia, S.; Xie, C.; Kong, Q.; Yu, S.; Lin, T.; Aloni, S.; Fakra, S.; Yang, P. Electrochemically scrambled nanocrystals are catalytically active for CO₂-tomulticarbonates. *Proc. Natl. Acad. Sci. U.S.A.* **2020**, *117*, 9194–9201.
- (9) Kim, D.; Kley, C. S.; Li, Y.; Yang, P. Copper Nanoparticle Ensembles for Selective Electroreduction of CO₂ to C₂-C₃ products. *Proc. Natl. Acad. Sci. U.S.A.* **2017**, *114*, 10560–10565.
- (10) Holtz, M. E.; Yu, Y.; Gao, J.; Abruña, H. D.; Muller, D. A. *In Situ* Electron Energy-Loss Spectroscopy in Liquids. *Microsc. Microanal.* **2013**, *19*, 1027–1035.
- (11) de Jonge, N.; Houben, L.; Dunin-Borkowski, R. E.; Ross, F. M. Resolution and Aberration Correction in Liquid Cell Transmission Electron Microscopy. *Nat. Rev. Mater.* **2019**, *4*, 61–78.
- (12) Khelifa, A.; Byun, C.; Nelayah, J.; Wang, G.; Ricolleau, C.; Alloyeau, D. Structural Analysis of Single NPs in Liquid by Low-Dose STEM Nanodiffraction. *Micron* **2019**, *116*, 30–35.
- (13) Karakulina, O. M.; Demortiere, A.; Dachraoui, W.; Abakumov, A. M.; Hadermann, J. *In Situ* Electron Diffraction Tomography Using A Liquid-Electrochemical Transmission Electron Microscopy Cell for Crystal Structure Determination of Cathode Materials for Li-Ion Batteries. *Nano Lett.* **2018**, *18*, 6286–6291.
- (14) Serra-Maia, R.; Kumar, P.; Meng, A. C.; Foucher, A. C.; Kang, Y.; Karki, K.; Jariwala, D.; Stach, E. A. Nanoscale Chemical and Structural Analysis during *In Situ* Scanning/Transmission Electron Microscopy in Liquids. *ACS Nano* **2021**, *15*, 10228–10240.
- (15) Yang, Y.; Shao, Y.-T.; Lu, X.; Yang, Y.; Ko, H.-Y.; DiStasio, R. A.; DiSalvo, F. J.; Muller, D. A.; Abruña, H. D. Elucidating Cathodic Corrosion Mechanisms with *Operando* Electrochemical Transmission Electron Microscopy. *J. Am. Chem. Soc.* **2022**, *144*, 15698–15708.
- (16) Holtz, M. E.; Yu, Y.; Gunceler, D.; Gao, J.; Sundararaman, R.; Schwarz, K. A.; Arias, T. A.; Abruña, H. D.; Muller, D. A. Nanoscale Imaging of Lithium Ion Distribution during *In Situ* Operation of Battery Electrode and Electrolyte. *Nano Lett.* **2014**, *14*, 1453–1459.
- (17) Yang, Y.; Shao, Y.-T.; Lu, X.; Abruña, H. D.; Muller, D. A. Metal Monolayers on Command: Underpotential Deposition at Nanocrystal Surfaces: A Quantitative *Operando* Electrochemical Transmission Electron Microscopy Study. *ACS Energy Lett.* **2022**, *7*, 1292–1297.
- (18) Egerton, R. F.; Cheng, S. C. Measurement of Local Thickness by Electron Energy-Loss Spectroscopy. *Ultramicroscopy* **1987**, *21*, 231–244.
- (19) Yang, Y.; Roh, I.; Louisia, S.; Yu, S.; Chen, C.; Jin, J.; Yu, S.; Salmeron, M. B.; Wang, C.; Yang, P. *Operando* Resonant Soft X-ray Scattering Studies of Chemical Environment and Interparticle Dynamics of Cu Nanocatalysts for CO₂ Electroreduction. *J. Am. Chem. Soc.* **2022**, *144*, 8927–8931.
- (20) Tate, M. W.; Purohit, P.; Chamberlain, D.; Nguyen, K. X.; Hovden, R.; Chang, C. S.; Deb, P.; Turgut, E.; Heron, J. T.; Schlom, D. G.; Ralph, D.; Fuchs, G. D.; Shanks, K. S.; Philipp, H. T.; Muller, D. A.; Gruner, S. M. High Dynamic Range Pixel Array Detector for Scanning Transmission Electron Microscopy. *Microsc. Microanal.* **2016**, *22*, 237–249.
- (21) Chen, Z.; Jiang, Y.; Shao, Y.-T.; Holtz, M. E.; Odstrcil, M.; Guizar-Sicairos, M.; Hanke, I.; Ganschow, S.; Schlom, D. G.; Muller, D. A. Electron Ptychography Achieves Atomic-Resolution Limits Set by Lattice Vibrations. *Science* **2021**, *372*, 826–831.
- (22) Li, F.; et al. Interplay of Electrochemical and Electrical Effects Induces Structural Transformations in Electrocatalysts. *Nat. Catal.* **2021**, *4*, 479–487.
- (23) Sun, K.; Yu, K.; Fang, J.; Zhuang, Z.; Tan, X.; Wu, Y.; Zeng, L.; Zhuang, Z.; Pan, Y.; Chen, C. Nature-Inspired Design of Molybdenum-Selenium Dual-Single-Atom Electrocatalysts for CO₂ Reduction. *Adv. Mater.* **2022**, *34*, 2206478.
- (24) Liu, C.; Wu, Y.; Sun, K.; Fang, J.; Huang, A.; Pan, Y.; Cheong, W.-C.; Zhuang, Z.; Zhuang, Z.; Yuan, Q.; Xin, H. L.; Zhang, C.; Zhang, J.; Xiao, H.; Chen, C.; Li, Y. Constructing FeN₄/graphitic Nitrogen Atomic Interface for High-Efficiency Electrochemical CO₂ Reduction over a Broad Potential Window. *Chem.* **2021**, *7*, 1297–1307.
- (25) Grosse, P.; Yoon, A.; Rettenmaier, C.; Herzog, A.; Chee, S. W.; Roldan Cuenya, B. Dynamic Transformation of Cubic Copper Catalysts during CO₂ Electroreduction and its Impact on Catalytic Selectivity. *Nat. Commun.* **2021**, *12*, 6736.
- (26) Walker, N. L.; Dick, J. E. Leakless, Bipolar Reference Electrode: Fabrication, Performance and Miniaturization. *Anal. Chem.* **2021**, *93*, 10065–10074.
- (27) Unocic, R. R.; Sacci, R. L.; Brown, G. M.; Veith, G. M.; Dudney, N. J.; More, K. M.; Walden, F. S., II; Gardiner, D. S.; Damiano, J.; Nackashi, D. P. Quantitative electrochemical measurements using *in situ* EC-S/TEM devices. *Microsc. Microanal.* **2014**, *20*, 452–461.
- (28) Yang, Y.; et al. Electrocatalysis in Alkaline Media and Alkaline Membrane-Based Energy Technologies. *Chem. Rev.* **2022**, *122*, 6117–6321.
- (29) Beermann, V.; Holtz, M. E.; Padgett, E.; de Araujo, J. F.; Muller, D. A.; Strasser, P. Real-Time Imaging of Activation and Degradation of Carbon Supported Octahedral Pt-Ni Alloy Fuel Cell Catalysts at the Nanoscale Using *In Situ* Electrochemical Liquid Cell STEM. *Energy. Environ. Sci.* **2019**, *12*, 2476–2485.
- (30) Sacci, R. L.; Black, J. M.; Balke, N.; Dudney, N. J.; More, K. L.; Unocic, R. R. Nanoscale Imaging of Fundamental Li Battery Chemistry: Solid-Electrolyte Interphase Formation and Preferential Growth of Lithium Metal Nanoclusters. *Nano Lett.* **2015**, *15*, 2011–2018.